PNAS

# Supporting information for

Neuronal PAS domain 1 identifies a major subpopulation of wakefulness-promoting GABAergic neurons in the basal forebrain.

Timothy A. Troppoli[1], Chun Yang[1, 2], Fumi Katsuki[1], David S. Uygun[1], Ilyan Lin[3], David Aguilar[1], Tristan Spratt[1], Radhika Basheer[1, 2], James M. McNally[1, 2], C. Savio Chan[4], James T. McKenna[1, 2*], Ritchie E. Brown[1, 2*§]

*****Equal Contribution

**Affiliations:**
[1] Laboratory of Neuroscience, VA Boston Healthcare System and Harvard Medical School, Dept. of Psychiatry, 1400 VFW Parkway, West Roxbury, MA, 02132, USA.
[2] Boston VA Research Institute, Boston, MA, 02130, USA.
[3] Wheaton College, Norton, MA, 02766, USA.
[4] Department of Neuroscience, Feinberg School of Medicine, Northwestern Univ., Chicago, IL, USA.

[§]**Corresponding author:**
Ritchie E. Brown, Dr. Rer. Nat.,
Address: Dept. of Psychiatry, VA Boston Healthcare System & Harvard Medical School, VA Medical Center, West Roxbury, 1400 VFW Parkway, MA, 02132, USA.
Email: Ritchie.Brown@va.gov; Ritchie_Brown@hms.harvard.edu

**This pdf file includes:**

## SI Materials and Methods

**Animals.** Npas1-cre-2A-tdTomato mice were provided by C. Savio Chan to establish a colony at VA Boston Healthcare System. The generation and validation of these mice, which are also available at Jackson Laboratory as strain 027718, has been previously described (1). Male hemizygous Npas1-cre-2A-tdTomato mice were crossed with female wild-type C57/BL6J mice (Jackson Laboratory strain 000664) mice to generate hemizygous mice for experiments. Genotype was verified by genotyping (Transnetyx, TN, USA). To identify BF vGlut1+ or vGlut2+ glutamatergic neurons, we crossed vGlut1-cre (Strain 023527; Jackson Laboratory) or vGlut2-cre mice (Congenic strain 028863; Jackson Laboratory) with a Cre-reporter strain expressing a red fluorescent marker (tdTomato; Strain 007905; Jackson Laboratory) to generate vGlut1-cre-tdTomato or vGlut2-cre-tdTomato mice respectively. The selective expression of Cre in vGlut1-cre mice has been validated previously (2). The selective expression of Cre-driven reporters in vGlut2 neurons when crossed with vGlut2-cre mice has also been validated in many brain areas (3, 4), including BF (5, 6). To identify BF GABAergic neurons, we used heterozygous GAD67-GFP knock-in mice (7-9) from our in-house colony. Male, heterozygous GAD67-GFP mice on a Swiss-Webster background were crossed with female wild-type Swiss-Webster mice. To test if there was co-localization of NPAS1 in GABAergic neurons, we crossed Npas1-cre-2A-tdTomato animals with GAD67-GFP animals and performed immunohistochemical staining for NPAS1 in GAD67-GFP mice. Both male and female animals were used for anatomical and sleep-wake experiments. We did not observe any obvious sex differences. Thus, results from male and female animals were pooled.

Mice were housed under constant temperature and a 12:12 light:dark cycle (7AM:7PM), with food and water available *ad libitum*. All experiments conformed to U.S. Veterans Administration, Harvard University, and U.S. National Institutes of Health guidelines on the ethical use of animals. All measures were taken to minimize the number of animals used and their suffering and experiments were carried out in accordance with the National Institute of Health Guide for the Care and Use of Laboratory Animals (NIH Publications No. 80-23). Experimental procedures were approved by the Institutional Animal Care and Use Committee (IACUC) of the VA Boston Healthcare System.

**Target area within the BF.** Our target area in the BF for neuronal characterization, anterograde tracing and chemogenetic experiments was the same as in our previous studies (6, 9, 10). We focused on intermediate areas of BF (horizontal limb of the diagonal band (HDB), magnocellular preoptic nucleus (MCPO), substantia innominata (SI) and ventral pallidum (VP)), where previous studies in the rat (11-13) and mouse (5, 14) found neurons projecting to the neocortex, approximately centered in BF at AP +0.14 mm; ML 1.6 mm; and DV -5.3mm. In contrast to our previous anatomical studies (6, 9) which were based on the Franklin and Paxinos 2008 mouse brain atlas (15), we used semi-automated analyses based on the Allen Brain Atlas to facilitate throughput and comparison with other studies. This brain atlas combines the SI and VP subregions into one area and as such we use the term SI/VP to refer to this subregion of BF. As noted in the main text, there are also other subtle differences of the boundaries of BF subregions, when comparing the Allen Brain Atlas with that of Frankin and Paxinos (15). Our analysis did not include the rostral aspect of BF (medial septum, vertical limb of the diagonal band (MS/DBV)), containing neurons largely projecting to the hippocampus, although $Npas1^{+}$ neurons were also present in these areas. We also did not include the most caudal aspect of the cholinergic BF which extends into and intermingles with neurons in the GPe since the anatomy and physiology of $Npas1^{+}$ neurons in the GPe have been extensively characterized in previous studies (1, 16).

**General methods for anatomical studies.** Mice were deeply anesthetized with sodium pentobarbital (50 mg/ml), exsanguinated with saline and perfused transcardially with a solution of 10% buffered formalin. Brains were post-fixed for 2 days in 10% formalin, and then transferred to a 30% sucrose solution for at least 24 hrs at 4ºC. Tissue was cut at a thickness of 40 µm on a freezing microtome and collected into four wells of PBS. Following all immunohistochemistry procedures, tissue was washed and mounted onto gelatin-coated slides, dried, and coverslipped using Vectashield Vibrance antifade hard set mounting medium with DAPI, or without DAPI when blue secondary antibodies were used (H-1800 and H-1700; Vector Laboratories, Inc., Burlingame, CA).

**Immunohistochemistry methods.** Prior to all immunohistochemical stains, coronal sections from one well were washed with PBS and placed in a blocking solution for one hour (0.5%

TritonX-100 in 1X PBS + 3% normal donkey serum (NDS)). All primary antibody solutions were made in PBS with 0.3% Triton X-100 and 1% NDS, and secondary solutions in PBS and 1% NDS. The tissue was rinsed twice with phosphate buffered saline (5 mins/rinse) between primary and secondary antibody incubations. Details of the primary and secondary antibodies are provided in **Supplemental Tables 3 and 4**. Npas1-cre-2A-tdTomato mice express tdTomato constitutively but at low levels (1)(**Supplemental Fig. 1A**). Thus, anti-RFP staining was used to enhance the red signal. Rabbit primary anti-RFP (anti-DsRed Living Colors, 632496, Takara, Mountain View, CA, 1:1000) was followed with donkey anti-rabbit AF594 (715-586-152, Jackson, 1:100). To identify *neurons* expressing $Npas1^+$ protein we used a previously described antibody (1) raised in guinea-pig (anti-NPAS1, 1:1000; validated in Npas1 knockout mouse tissue) followed by either donkey anti-guinea pig AF488 (706-545-148, Jackson, 1:500) or AF594 (706-585-148, Jackson, 1:500) for 2 hours at room temperature. To identify *cholinergic neurons* tissue was incubated in rabbit anti-choline acetyltransferase (ChAT, the synthetic enzyme for acetylcholine) for three days at 4ºC (1:150; Cat#AB143, EMD Millipore, Billerica, MA) followed by incubation in a secondary antibody coupled to a green (donkey anti-rabbit AF488, Cat#A21206, Thermo Fisher Scientific, Cambridge, MA) fluorophore for 3 hrs at room temperature (1:200; RT). To identify *parvalbumin (PV)* neurons, tissue was incubated in sheep anti-PV overnight at 4ºC (1:150; Cat#AF5058, RnD Systems, Minneapolis, Mn) followed by a secondary antibody (1:200) coupled to a green (donkey anti-sheep AF488 Cat#A11015, Thermo Fisher Scientific) fluorophore for 3 hrs at RT. To *amplify EYFP* signal for anterograde tracing using AAV5-DIO-ChR2-EYFP, tissue was incubated in mouse polyclonal anti-GFP primary antibody (1:300; Cat#MAB3580, EMD Millipore) for 3 days at 4°C, and secondary antibody (1:500; donkey anti-mouse AF488, Cat#A21202, Thermo Fisher Scientific) overnight (16 hrs) at 4ºC. To identify neurons which were activated during chemogenetic experiments where $Npas1^+$ neurons were identified by the presence of mCherry (red) we performed immunohistochemical staining for the immediate early gene cFOS, using a primary antibody raised in rabbit (1:200 overnight at 4ºC; EMD Millipore Cat#ABE457) followed by donkey anti-rabbit secondary antibody (1:200 for 2hrs at RT; Thermofisher Cat#A-21206;) conjugated to a green fluorophore (AF488). To identify $ChAT^+$ or $PV^+$ neurons in tissue with mCherry (red) and cFOS stained-AF488 (green) neurons/nuclei, we incubated the tissue with the primary antibodies against ChAT and PV described above with a blue secondary antibody (donkey anti-rabbit AF350,

Cat#A10039, Thermo Fisher Scientific; 1:200) or (donkey anti-sheep AF350, 1:200, Cat#A21097, Thermo Fisher Scientific) for 3 hrs at room temperature. All primary (**Supplemental Table 3**) and secondary (**Supplemental Table 4**) antibodies used here have been previously validated and used in peer reviewed publications. Secondary antibody-only controls were also performed, omitting the above-listed primary antibodies.

**AAV5-DIO-ChR2-EYFP injection for anterograde tracing of the projections of BF Npas1$^{+}$ neurons.** Viral vectors encoding Channelrhodopsin-2 (ChR2) and enhanced yellow fluorescent fusion proteins (AAV5-DIO-ChR2-EYFP) originally generated by the laboratory of Dr. Karl Deisseroth (Stanford University, CA, USA) were purchased from the University of North Carolina Vector Core facility. Mice were deeply anesthetized with isoflurane (1-3%) and viral injections were performed using a 1 µl Hamilton syringe (Cat#87900, Point Style 2, Hamilton Company, Reno, NV, USA), targeting BF (AP +0.14 mm; ML 1.6 mm; DV -5.3mm). 300 nl of viral vector was injected unilaterally at a flow rate of 50 nl/min. The needle was left in place for an additional 10 mins to allow virus diffusion in the brain and to avoid backflow along the needle tract. Once viral injections were complete, the needle was slowly removed. Animals were sacrificed following one month of survival post-injection.

**Chromophore co-localization quantification/photographic depiction.** For each fluorophore, representative BF sections (three 40 µm coronal sections per animal, spanning +0.38 mm (rostral), +0.14 mm (medial), and -0.10 mm (caudal) from bregma)) were imaged using StereoInvestigator and quantified using NeuroInfo software packages (Version 2022; Microbrightfield, Williston, VT) and a Zeiss Imager.M2 fluorescent microscope. Neurons labeled with tdTomato or RFP were identified by the presence of red (excitation:emission at 590:617 nm) fluorescence in the cytoplasm and nucleus. Neurons labeled with GFP/green secondary antibody or a blue secondary antibody were identified by were identified by the presence of green or blue (excitation:emission 488:509 nm and 343:441 nm, respectively) fluorescence in the cytoplasm (PV or ChAT stains) or nucleus (cFOS or NPAS1 IHC stains). Green staining was observed in the cytoplasm and nucleus for GAD67-GFP mice, as in our previous studies (6, 9, 10). There was a high background level of GFP in the neuropil due to the presence of GFP in GABAergic fibers, particularly in the dorsal BF. In our previous studies

using these mice (6, 9), non-GABAergic neurons, i.e. $ChAT^+$ or $vGlut2^+$ neurons, demonstrated GFP fluorescence which was below background levels, and we used the same criterion to identify GFP-negative nuclei here.

The BF region of each section was roughly traced under low (5X) magnification. The 3D Slide Scanning Workflow feature of StereoInvestigator was then used to capture and stitch together individual Z-stacks taken within the outlined BF region at a higher (10X) magnification. Each stack was comprised of 8 focal planes between the top and bottom of the tissue slice, manually determined at upper and lower stage height boundaries where clear focus is lost. Once a composite Z-stack of the entire BF was taken, the image was then collapsed to a single plane using the Deep Focus feature in NeuroInfo to visualize cells and nuclei throughout the depth of the section. An initial pass at quantification was automatically performed using the Cell Detection function of NeuroInfo, which identifies fluorescent puncta from size and intensity. To reduce false positives, diameters were conservatively set between 5-7 μm for nuclear stains and 10-15 uM for cytoplasmic stains. Automatically detected cells were manually confirmed and additional quantification within the BF was manually performed as needed for additional undetected neurons. Colocalization was first assessed automatically by distance (≤7 μm between labeled puncta) and confirmed by manual inspection.

After cells in the BF were labeled, the Section Registration function of NeuroInfo was used to align the captured image to its corresponding plane in the 3D Allen Mouse Brain Atlas, correcting for the sectioning angle and any skew in X and Y dimensions resulting from mounting or post-fixation distortion. Regions of interest (SI/VP, HDB, MCPO, and surrounding areas) were plotted onto the section image, and the total number of marked cells in each region was then exported. Cell density was calculated by dividing the total number of cells in each subregion by its area in $\mu m^2$.

Long-axis measurement. The long-axis diameter of Npas1-tdTomato labeled neurons was measured for each of the 3 BF subnuclei using NeuroInfo software and images collected as described above. 10 neurons per BF subnuclei (HDB, MCPO, SI/VP, 5 neurons/hemisphere) were randomly selected and measured for the 3 representative sections (rostral, intermediate, and caudal) in each animal.

Anterograde tracing. EYFP fluorescence in mice injected with AAV5-DIO-ChR2-EYFP was first amplified with anti-GFP antibody and secondary antibody conjugated to a green

fluorophore. 40 µm coronal sections were mounted, incorporating tissue from the most rostral to most caudal sections and spaced 80 µm apart, anatomically. Whole-slide scans were performed at 20x magnification utilizing the PhenoImager HT automated multispectral imaging system (Akoya Bioscience, Marlborough, MA). BF Npas1$^{+}$ efferent regions (AAV-EYFP anterograde projections) were identified as regions where varicosities of AAV-EYFP-labeled axons were located. The relative abundance of individual projections was agreed upon by 2 or more experimenters.

**Chemogenetics and stereotaxic surgery.** To test the effect of activation of BF Npas1$^{+}$ neurons on sleep-wake behavior, adeno-associated viral vectors expressing excitatory receptors and a fluorescent marker of expression (AAV8-hSyn-DIO-hM3D(Gq)-mCherry, plasmid #44361, Addgene, Watertown, MA) were injected bilaterally into BF (AP: + 0.14, ML: ± 1.6, DV: -5.3) at 0.5, 0.7 or 1 µl/side of adult (3-6 month old) mice. The number of neurons transduced, and sleep-wake effects, were comparable among the different doses and have been pooled. To record cortical electrical activity, bilateral frontal neocortical EEG screw electrodes (Pinnacle Technology Inc.; Kansas, United States; Part # 8403) were placed at AP: +1.9 mm, ML: ± 1.5 with a ground electrode at AP: -3 mm, ML: +2.7 and a reference electrode at AP: -5.2 mm ML: 0. Electrodes were soldered to a headmount (Pinnacle Technology Inc.; Part # 8201-SS). EMG electrodes were placed in the nuchal muscle. All chronically implanted components were secured with dental cement (Keystone industries, Bosworth Fastray; Part # 0921378). Four or more weeks later (to allow for viral transduction), sleep-wake recordings began at 7AM (ZT0). Intraperitoneal injections of saline (vehicle control) or 0.3 or 1 mg/kg CNO (Sigma-Aldrich, #C0832, diluted to 0.1 mg/mL) were given early in the light cycle at 9AM (ZT2) when mice normally sleep, as we predicted an increase in wakefulness based on previous results investigating all BF GABAergic neurons (5). Control CNO injection experiments were conducted in a different strain of transgenic mice (Lhx6-cre) on the same C57/BL6J background strain of mice using a control virus expressing a fluorescent marker without hM3d(Gq) (AAV-DIO-EYFP). Following completion of sleep-wake recordings and 120 min prior to sacrifice, mice received an additional injection of saline or CNO (0.3 or 1 mg/kg) at ZT2 to verify activation of Npas1$^{+}$ neurons using immunohistochemical staining for the immediate early gene cFOS.

**Sleep-wake recordings and analysis.** Prior to beginning experiments, mice were tethered and acclimatized to the recording chamber for at least 3 days. After acclimatization, continuous EEG/EMG (8200-K1-SL amplifier; Pinnacle Technology Inc., Lawrence, KS, USA) recordings were performed before, during, and after i.p. injections of CNO or saline (vehicle control) for 24 hrs from ZT0-24. EEG/EMG were recorded using Sirenia Sleep Pro (Pinnacle Technology). EEG signals were acquired at 1 kHz with a 0.5Hz high-pass hardware filter, amplified 100x and bandpass filtered at 0–500 Hz. EMG signals were filtered at 0-100 Hz. As previously described (17, 18), sleep-wake states were manually scored in 4 s epochs as follows: An epoch was considered *wakefulness* when the EEG showed a desynchronized low amplitude signal together with high muscle tone in the EMG signal; the large EMG signal did not need to be phasic in appearance to be characterized as wakefulness. An epoch was considered non-rapid-eye-movement (NREM) sleep when the EEG signal showed large amplitude, slow synchronized waves, and a low amplitude EMG signal, except for very brief bursts which were considered twitching. An epoch was considered REM sleep when the EEG signal presented a repetitive stereotyped 'sawtooth' signal in the theta range (4-9 Hz), with a nearly flat EMG signal. Epochs with artifacts such as wake epochs where the EEG was contaminated by crosstalk with EMG signals, or periods of NREM or REM sleep with large amplitude DC shifts were excluded for analyses of EEG signals, i.e. power spectral density. Scoring was performed in Sirenia Sleep, and EEG signals and scored epochs were exported for further analysis in MATLAB.

Power spectral densities of wake, NREM sleep, and REM sleep were computed using the MATLAB pwelch function using a 4-second Hanning window with 50% overlap. Frequency bands were defined as follows: slow wave: 0-1.5 Hz; delta: 1.5-4 Hz; theta: 4-9 Hz; alpha/sigma: 9-15 Hz; beta: 15-30 Hz; gamma: 30-80 Hz. To normalize EEG power, power in each of these frequency bands per state was divided by the total power across all frequencies (0-500Hz) from the entire 24 hr record. Power spectra were binned in 3-hour intervals, except for the NREM sleep delta power time course throughout the light cycle (**Supplemental Figure 5B**), which used 1-hour bins. Normalized power per state per band was averaged within treatment groups. We analyzed sleep spindles (≥0.5 s in length) using our validated automated spindle detection algorithm (19)(https://osf.io/2ne8j/), where normalized amplitude is calculated by dividing against a threshold value based on putative spindle peaks in each EEG record. Representative

time-frequency multi-taper spectrograms were created using the mtspectrogramc function (Chronux Toolbox; Chronux.org)(20).

Bout durations were binned into discrete intervals, summed, and presented as a percentage of total time in the state. Latency to NREM sleep was defined as the time post-injection until the start of 10 continuous NREM sleep epochs (40 s). Latency to REM sleep was defined as the time post-injection until the start of 5 continuous REM sleep epochs (20 s). Brief awakenings were defined as a ≤ 4 epoch (≤ 16 s) long period of wake interrupting 2 NREM sleep epochs.

*Statistical Analysis*

Data are presented as mean ± SEM. Outliers were identified using Grubb's outlier test at a threshold of $p<0.005$ or less, and reported when excluded. All neuroanatomical density, long-axis diameter, co-localization measures, and comparisons of group averages (i.e. average sleep latencies or spindle densities) were analyzed using one-way analysis of variance (ANOVA), to compare differences between BF subnuclei (HDB, MCPO, SI/VP), coronal BF section representations (rostral, medial, and caudal), or drug treatments. Two-way ANOVAs were performed to analyze treatment effects over time. When appropriate in an individual ANOVA analysis, repeated-measures (RM) factor-matching was performed. If a main effect of the ANOVA was significant, pair-wise comparisons between groups were then made, using Holm-Šídák multiple comparison corrections. NREM sleep spindle analyses over time were performed using two-way mixed-model ANOVAs to facilitate RM two-factor analyses when individual datapoints within subjects were excluded (i.e. a mouse exhibited no NREM sleep during a particular bin). Comparisons between 2 group means were performed as two-tailed t-tests and paired when appropriate. Cumulative histograms are compared as two-sample Kolmogorov-Smirnov (K-S) tests. Statistics were performed in GraphPad Prism (Version 9.X and 10.X, GraphPad Software, Boston, MA), MATLAB (Version 2023a, The MathWorks Inc, Natick, MA) or Microsoft Excel (Version 2016, Microsoft, Redmond, WA).

**Supplemental Figures –**

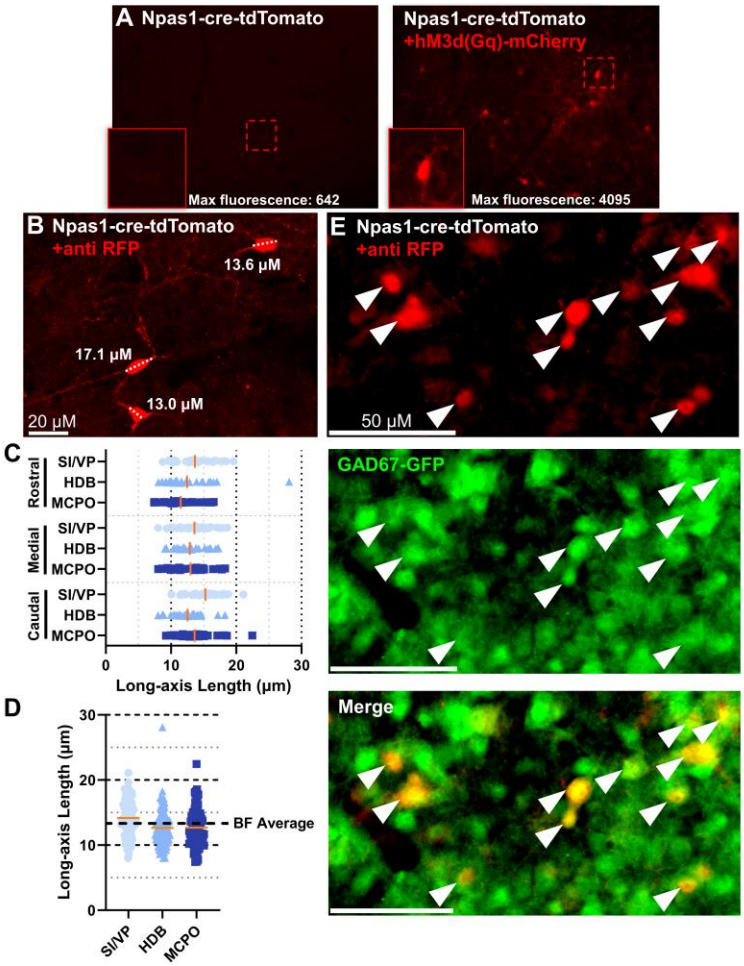


**Fig. S1. Basal forebrain (BF) neuronal PAS domain 1 (Npas1+) cells are small or medium sized neurons and colocalize with glutamic acid decarboxylase 67kDa (GAD67)-expressing cells in a GAD67-GFP/Npas1-cre-2A-tdTomato mouse genetic cross. (A)** Npas1-cre-tdTomato cells express minimal tdTomato fluorescence without immunohistochemical amplification. This background expression does not hinder the visual identification of neurons transduced with hM3D(Gq)-mCherry. Maximal fluorescence for endogenous tdTomato and virally transduced mCherry for a sample cell (outlined, inset) within the same section and taken with the same exposure/gain parameters is listed as a 12-bit red-channel intensity value (range: 0-4095). **(B)** Example subset of BF Npas1-tdTomato neuron long-axis measurements. Note: As quantified in **Fig. 1F**, tdTomato+ neurons reflect adult Npas1+ neurons (~75%), as well as those that expressed Npas1 during development but no longer have NPAS1 protein detectable by immunohistochemistry (~25%). **(C)** Distribution of Npas1-tdTomato long-axis measurements from a random selection of 10 cells per BF subregion across rostral, medial, and caudal BF sections collected from each of 3 animals (270 cells total). Mean long-axis measurement per subregion is marked with an orange line. **(D)** Npas1-tdTomato cells were significantly longer in rostral vs. ventral BF subregions (Substantia innominata/ventral pallidum, SI/VP: 14.17 ± 0.35 µm, vs. Horizontal limb of diagonal band, HDB: 12.63 ± 0.55 µm, p=0.0010; Magnocellular Preoptic area, MCPO: 12.70 ± 0.39 µm, p=0.0012, mean marked by an orange line. The overall length of Npas1-tdTomato cells in the BF was 13.2 ± 0.4 µm, indicated by a dashed black line.

Comparisons made via one-way ANOVA (p=0.0003). **(E)** Example image within the BF showing colocalization of Npas1-tdTomato cells (red) with GAD67-GFP cells (green) following a GAD67-GFP/Npas1-cre-2A-tdTomato mouse cross. Colocalization is indicated with an arrowhead.

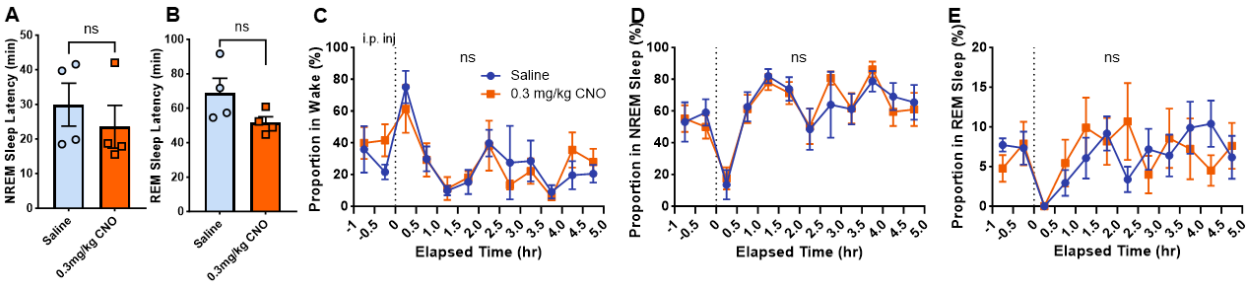


**Fig. S2**. Clozapine N-oxide (CNO) alone has no impact on sleep behavior in mice lacking expression of excitatory hM3D(Gq) receptors. **(A)** Latency to non-rapid-eye-movement (NREM) sleep is unchanged between saline and 0.3 mg/kg CNO administration (n=4, p=0.28, two-tailed paired t-test). **(B)** Latency to rapid-eye-movement (REM) sleep is also not significantly different between saline and 0.3 mg/kg CNO administration (n=4, p=0.17, two-tailed paired t-test). **(C)** The proportion of time spent awake was not significantly different between saline and 0.3 mg/kg CNO treated animals at any time point. Two-way ANOVA identifies no interaction between time x treatment ($F_{11,72}$ = 0.507 p=0.89). **(D)** Time spent in NREM sleep did not significantly differ between saline and 0.3 mg/kg CNO treated animals at any time point. Two-way ANOVA identifies no interaction between time x treatment ($F_{11,72}$ = 0.291 p=0.99). **(E)** The proportion of mice time spent in REM sleep was not significantly different between saline and 0.3 mg/kg CNO groups at any time point. Two-way ANOVA identifies no interaction between time x treatment ($F_{11,72}$ = 0.892 p=0.55). ns: not significant.

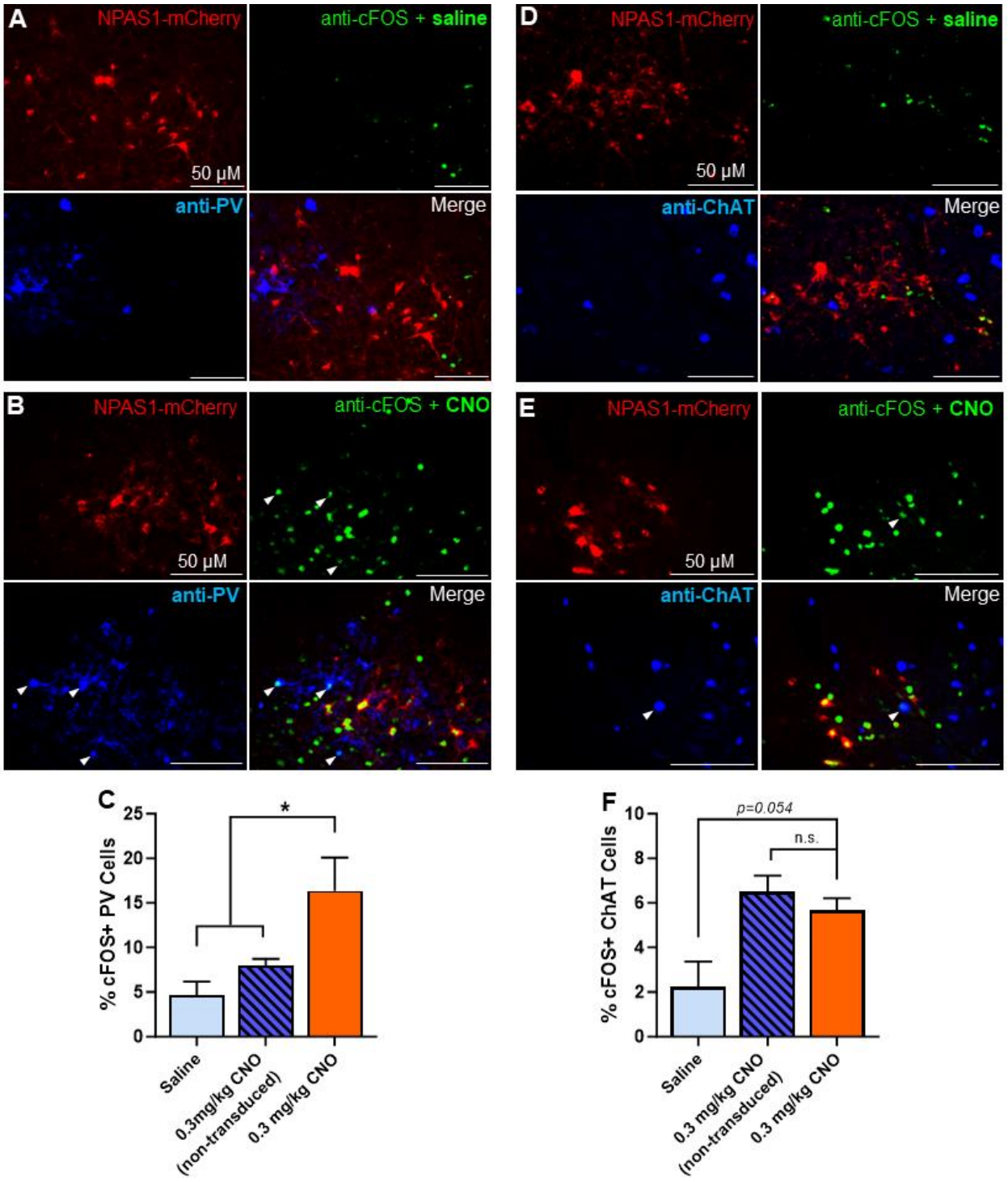


**Fig. S3.** Chemogenetic stimulation of basal forebrain (BF) neuronal PAS domain 1 (Npas1+) cells activates parvalbumin (PV) neurons consistent with their wake-active profile. **(A, B)** Representative immunohistochemically stained images depicting transduced Npas1-mCherry cells (red), an anti-cFOS nuclear stain (green), and a stain against PV cells (blue) collected from animals administered saline (A) or 0.3 mg/kg clozapine-N-oxide (CNO, B) 2h prior to sacrifice. Colocalized cFOS and PV puncta are labeled with an arrowhead. **(C)** Chemogenetic activation of

BF Npas1+ neurons with 0.3 mg/kg CNO increased double-labeling of all BF PV+ cells with an anti-cFOS nuclear stain compared to saline administration or CNO administration in mice lacking hM3Dq (for all, n=3 mice; saline 4.65% ± 1.53%, p=0.025; CNO in mice lacking hM3Dq 7.94 ± 0.77%, p=0.045; CNO in mice with Npas1 neurons transduced with hM3Dq 16.4% ± 3.72%. One way ANOVA, p=0.031). **(D, E)** Representative images depicting transfected Npas1-mCherry neurons (red), an anti-cFOS nuclear stain (green), and a stain against ChAT cells (blue) in BF tissue from animals given saline (D) or 0.3 mg/kg CNO (E) prior to sacrifice. cFOS and ChAT colocalization is marked with an arrowhead. **(F)** Administration of 0.3mg/kg CNO did not enhance the percentage of transduced BF Npas1+ neurons over non-transduced Npas1+ cells (n=3 mice; 6.51 ± 0.71% vs. 5.66% ± 0.55%, p=0.50) but tended to produce higher cFOS expression than saline administration alone (n=3 mice; 2.24% ± 1.13%, p=0.054; one-way ANOVA, p=0.024). *p<0.05, n.s. not significant.

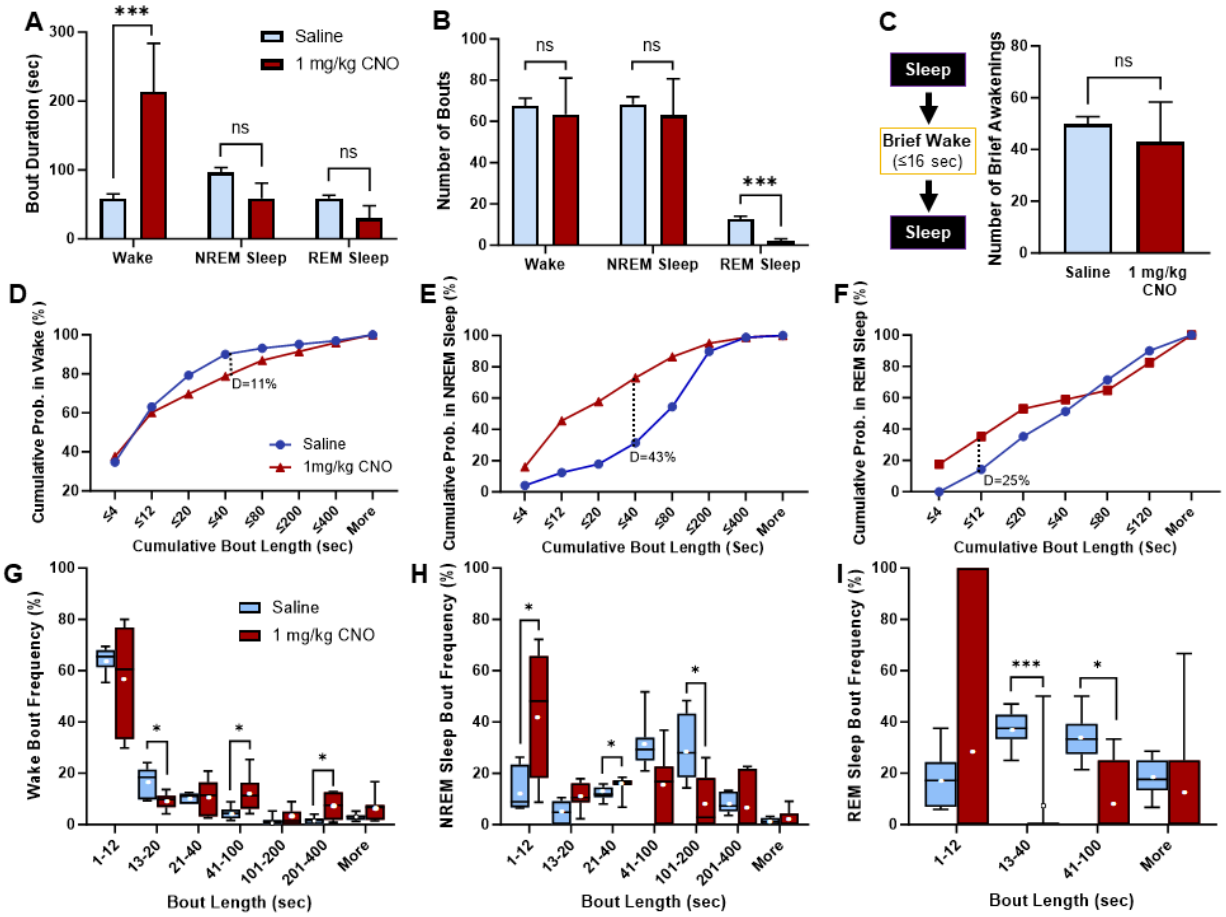


**Fig. S4. Chemogenetic activation of basal forebrain (BF) neuronal PAS domain 1 (Npas1+) neurons with 1 mg/kg clozapine-N-oxide (CNO) significantly lengthens wake bouts and suppresses the frequency of rapid-eye-movement (REM) sleep bouts**. **(A)** Compared to saline (n=7 mice), 1 mg/kg CNO (n=7) administration promotes significantly longer wake bouts over the 3-hour post-injection period (58.0 ± 7.1 s vs 213.2 ± 70.52 s respectively, p=0.0039; two-tailed paired t-test). Average non-rapid-eye-movement (NREM) sleep bout length was not significantly different following administration of saline compared to 1 mg/kg CNO (95.9 ± 7.6 sec vs 58.5 ± 22.2 sec respectively, p=0.14), nor was REM sleep bout length (58.9 ± 4.3 sec vs. 30.0 ± 18.2, p=0.15). **(B)** The number of wake bouts was not significantly different between saline and 1 mg/kg CNO administration during the 3-hour post-injection period (67.6 ± 3.7 vs. 63.4 ± 17.6 respectively, p=0.85), nor were the number of NREM sleep bouts (68.3 ± 3.7 vs. 63.0 ± 17.6, p=0.80). However, compared to saline, 1 mg/kg CNO administration produced significantly fewer REM sleep bouts (12.7 ± 1.3 vs. 2.0 ± 1.1, p=0.00056). **(C)** The number of brief awakenings (≤16 sec of wake interspersing 2 sleep bouts) was not significantly different between saline and 1 mg/kg CNO treatments (49.7 ± 3.0 vs. 42.9 ± 15.5, p=0.70). **(D)** A cumulative probability plot of wake bout lengths during the 3-hour post-injection period indicates 1 mg/kg CNO produces significantly fewer short wake bouts (p=0.0031, Kolmogorov-Smirnoff, K-S test D=0.11). **(E)** NREM sleep bout length cumulative distributions are significantly different between saline and 1 mg/kg CNO administrations, favoring shorter NREM sleep bouts (p<0.0001, D=0.43). **(F)** Cumulative distributions of REM sleep are not significantly different between treatments (p=0.30, K-S D=0.25). **(G)** Bout analysis finds significantly fewer

short wake bouts between 13-20 sec (p=0.045), and significantly more between 41-100 sec (p=0.039), and 201-400 sec (p=0.019) following 1 mg/kg CNO administration vs. saline. **(H)** 1 mg/kg CNO produces significantly more short-duration NREM sleep bouts between 1-12 sec (p=0.025) and 21-40 sec (p=0.024), and significantly fewer long bouts between 101-200 sec (p=0.019). **(I)** 1 mg/kg CNO administration produces significantly fewer REM sleep bouts between 13-40 sec (p=0.0041) and 41-100 sec (p=0.039). $p<0.05$ *, $p<0.005$ ***. ns: not significant. Cumulative histograms are compared as two-sample nonparametric K-S tests, and individual binned bout comparisons were made via two-tailed paired t-tests. Whiskers on box and whisker plots range from min to max, the midline represents the median, and the mean is indicated with a white circle. Up to 1 animal per group bin may be excluded if it is alone in spending 0% or 100% of its time in that bin. $p<0.05$ *, $p<0.01$ **, $p<0.005$ ***, ns: not significant.

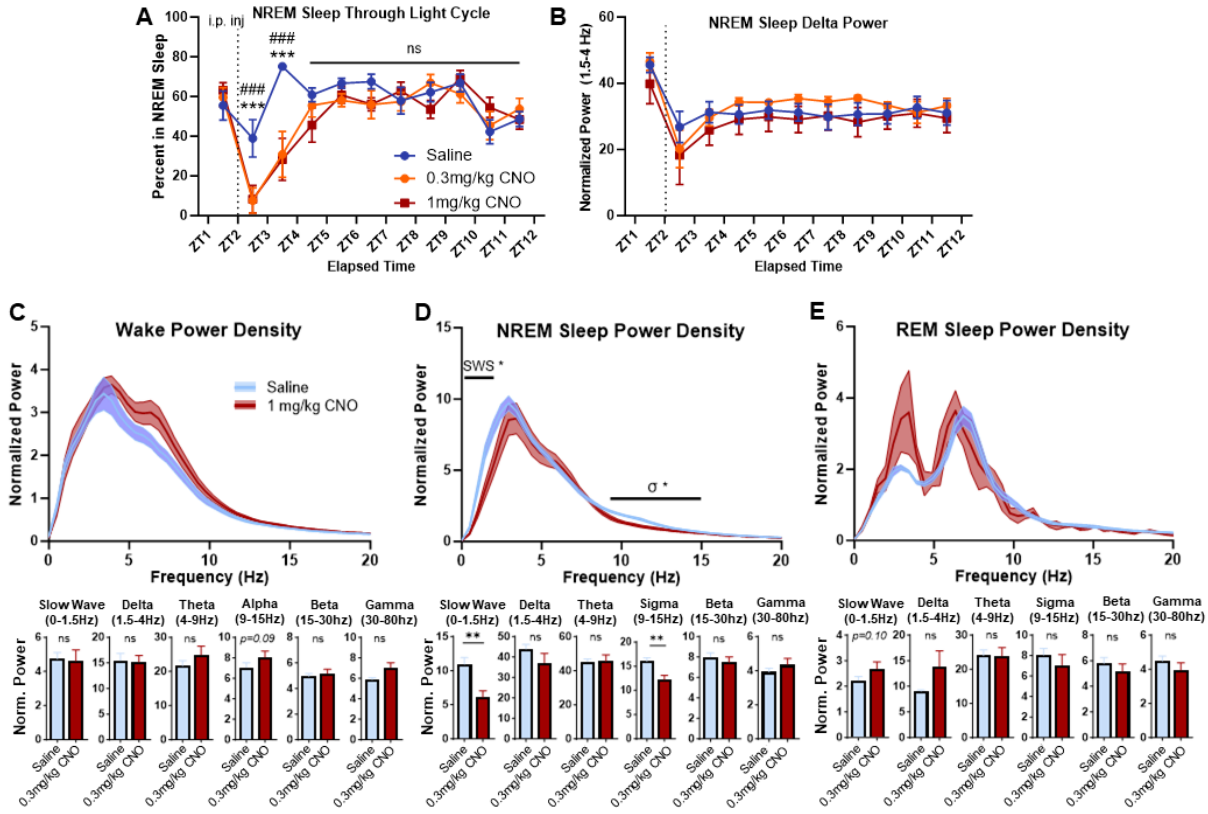


**Fig. S5. Chemogenetic activation of basal forebrain (BF) neuronal PAS domain 1 (Npas1+) neurons does not result in a rebound of non-rapid-eye-movement (NREM) sleep time or NREM delta power during the light period, but activation of BF Npas1+ neurons with 1 mg/kg clozapine-N-oxide (CNO) does significantly alter NREM sleep spectral EEG activity.** **(A)** Administration of 0.3 mg/kg (n=9) and 1 mg/kg CNO (n=7) suppresses NREM sleep compared to saline (n=9) for 2 hours post-injection. Afterwards, mice spend similar proportions of time in NREM sleep throughout the duration of the light cycle. Two-way ANOVA identifies a significant interaction of time x treatment ($F_{(20,198)} = 3.0$, $p<0.0001$). **(B)** There is no significant difference in NREM sleep delta power (1.5-4Hz) across treatments at any timepoint. Two-way ANOVA identifies no interaction of time x treatment ($F_{(20,171)} = 0.91$, $p=0.58$). **(C)** A normalized power density plot and power spectra analyses identifies a trend for higher wake alpha power (9-15Hz, maximally between 11.7-12.2Hz) following 1 mg/kg CNO (n=7) vs saline (n=7) administrations (p=0.090, comparisons made via two-tailed paired t-tests). No significant changes were observed in slow wave (p=0.95), delta (p=0.79), theta (p=0.17), beta (p=0.44) or gamma power bands (p=0.35). One animal's slow-wave wake data was identified as an outlier using Grubb's test ($p<0.001$) and was excluded from slow-wave calculations and the PSD plot. **(D)** Power density spectra for NREM sleep and normalized power band analysis indicates that 1 mg/kg CNO administration produces significant less power in the slow wave (0-1.5Hz, maximally at 0.49-0.98Hz, p=0.0086) and sigma power bands (9-15Hz, maximally at 10.7-11.2Hz, p=0.0094). No significant differences were seen in delta (p=0.19), theta (p=0.99), beta (p=0.44) or gamma bands (p=0.31). **(E)** Frequency spectra were not significantly different between treatments during REM sleep, though there was a trend toward increased slow-wave activity (p=0.099). Other bands showed no change, including delta (p=0.21), theta (p=0.74), sigma (p=0.65), beta (p=0.85), or gamma (p=0.70). $p<0.05$ *, $p<0.01$ **. ns: not significant.

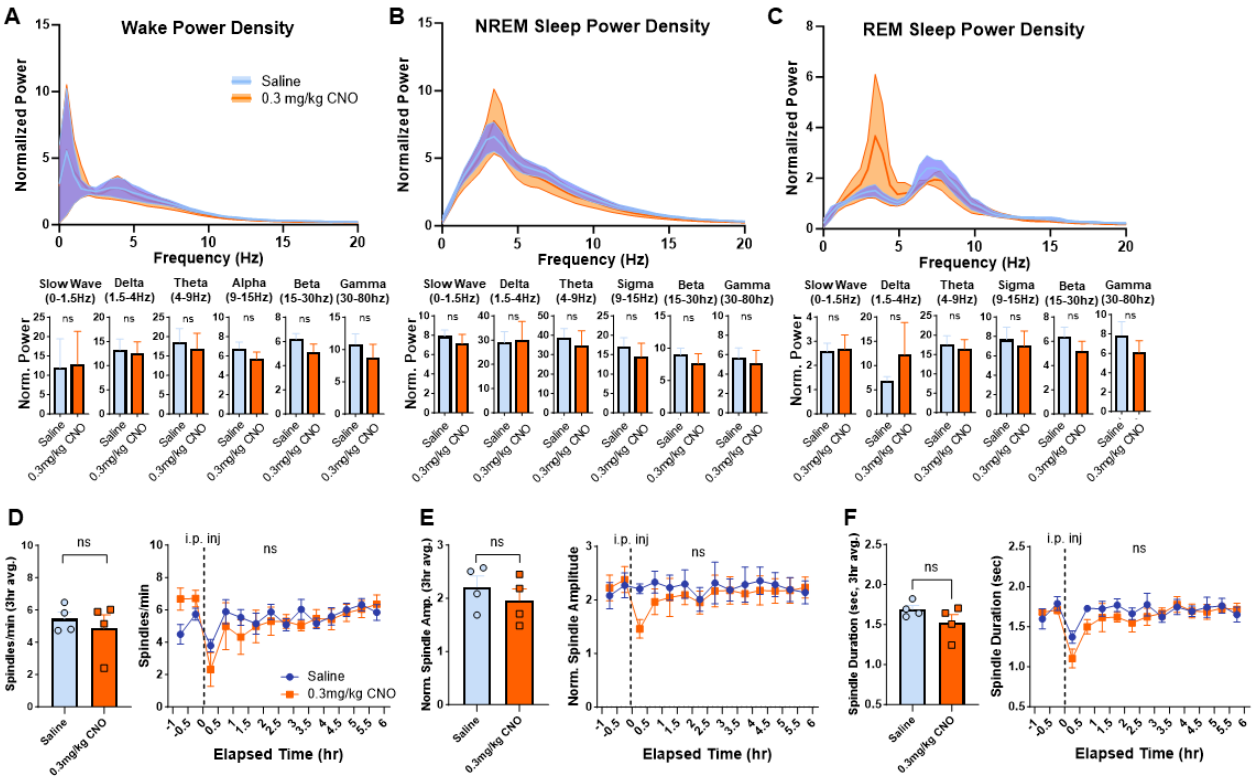


**Fig. S6. Clozapine-N-oxide (CNO) alone has no impact on cortical electroencephalogram (EEG) or sleep spindle activity. (A)** Without transduction of excitatory hM3D(Gq), administration of 0.3 mg/kg CNO (n=4) does not significantly change wake EEG power spectra compared to saline (n=4) across slow wave (0-1.5Hz, p=0.43), delta (1.5-4Hz, p=0.73), theta (4-9Hz, p=0.21), alpha (9-15Hz, p=0.19), beta (15-30Hz, p=0.14) or gamma bands (30-80Hz, p=0.31). Comparisons were made using two-tailed paired t-tests. **(B)** 0.3 mg/kg CNO alone does not significantly impact non-rapid-eye-movement (NREM) sleep EEG power spectra compared to saline at slow wave (p=0.33), delta (p=0.74), theta (p=0.27), sigma (p=0.13), beta (p=0.13), or gamma power bands (p=0.23). **(C)** Rapid-eye-movement (REM) sleep power spectra are not significantly impacted by 0.3 mg/kg CNO vs. saline administration at slow wave (p=0.89), delta (p=0.43), theta (p=0.73), sigma (p=0.57), beta (p=0.18), or gamma bands (p=0.16). **(D)** Over the 3-hour post-injection period, spindle density was not significantly different between saline (5.45 ± 0.42 spindle/min) or 0.3 mg/kg CNO (4.86 ± 0.84 spindle/min, two-tailed paired t-test p=0.40). There is no significant difference in spindle density between treatments at any timepoint following injection. Two-way ANOVA identifies no interaction of time x treatment ($F_{(13,74)}$ = 1.53, p=0.13). **(E)** Normalized spindle amplitude did not significantly differ between saline (2.21 ± 0.21) and 0.3 mg/kg CNO (1.96 ± 0.22, p=0.16). Spindle amplitude did not significantly differ at any point following injection, and two-way ANOVA identifies no interaction of time x treatment ($F_{(13,74)}$ = 1.77, p=0.09). **(F)** Additionally, spindle duration following saline administration (1.69 ± 0.049 s) was not significantly different than 0.3 mg/kg CNO treatment (1.52 ± 0.10 s, p=0.21). Spindle duration was not significantly different at timepoints following drug injection, and two-way ANOVA identifies no interaction of time x treatment ($F_{(13,74)}$ = 1.19, p=0.30). ns: not significant.

## Supplemental Tables

| Average Cell Density Per Region (cells/mm^2 ± SEM) | | | | |
|---|---|---|---|---|
| **BNST** | **MnPO** | **MPO** | **LPO** | **VLPO** |
| 105.81 ± 7.85 | 86.74 ± 40.86 | 105.64 ± 13.88 | 120.82 ± 19.02 | 26.04 ± 12.01 |
| (88.5 ± 2.1 cells) | (2.66 ± 1.2 cells) | (48.9 ± 5.2 cells) | (35.6 ± 7.8 cells) | (2.4 ± 1.1 cells) |

**Supplemental Table 1. Densities of Neuronal PAS domain 1 positive neurons surrounding the basal forebrain (BF).** BNST, bed nucleus of stria terminalis; LPO, lateral preoptic area; MnPO, Median preoptic area; MPO, medial preoptic area; VLPO, ventrolateral preoptic area. Note: the numbers of Npas1 neurons in the small MnPO and VLPO regions tended to be very low (<5/section). The MnPO region was not obvious in our caudal BF section and the small area of the region, along with inter-animal variations in cell count, magnified the density and variability within the MnPO.

| | Region | Ipsi- | Contra- |
|---|---|---|---|
| *Neocortical* | Agranular insular cortex (AI) | + | + |
| | Anterior cingulate area (ACA) | ++ | + |
| | Auditory cortex (AUD) | +/- | |
| | Claustrum (CLA) | + | |
| | Ectorhinal cortex (ECT) | + | |
| | Endopiriform nucleus (EP) | ++ | |
| | Gustatory cortex (Gu) | +/- | |
| | Infralimbic area (ILA) | ++ | + |
| | Motor cortex (MO) | + | + |
| | Orbital cortex (ORB) | + | |
| | Parietal cortex (PTL) | + | |
| | Perirhinal cortex (PERI) | + | |
| | Prelimbic cortex (PreL) | + | + |
| | Retrosplenial cortex (RSP) | ++ | + |
| | Somatosensory cortex (SS) | + | |
| | Temporal association area (TEA) | + | |
| | Visceral cortex (VISC) | +/- | |
| | Visual cortex (VIS) | + | |
| *Hippocampal* | Dentate gyrus (DG) | + | + |
| | Entorhinal cortex (ENT) | ++ | |
| | Field CA1 | + | + |
| | Field CA2 | +/- | +/- |
| | Field CA3 | + | + |
| | Subiculum, dorsal (SUBd) | ++ | + |
| | Subiculum, ventral (SUBv) | + | +/- |
| *Thalamic* | Anterodorsal thalamic nucleus (AD) | + | |
| | Anteromedial thalamic nucleus (AM) | + | |
| | Anteroventral thalamic nucleus (AV) | +/- | |
| | Centromedial thalamic nucleus (CM) | + | + |
| | Habenula, lateral (LH) | ++ | + |
| | Habenula, medial (MH) | + | +/- |
| | Interanteromedial thalamic nucleus (IAM) | + | + |
| | Intermediodorsal thalamic nucleus (IMD) | + | + |
| | Mediodorsal thalamic nucleus (MD) | +/- | |
| | Nucleus reuniens (RE) | + | + |
| | Parafascicular nucleus (PF) | +/- | |
| | Parataenial nucleus (PT) | + | |
| | Rhomboid nucleus (RH) | + | + |
| | Thalamic paraventricular nucleus (PVT) | ++ | + |
| | Thalamic reticular nucleus (TRN) | + | |
| | Ventromedial thalamic nucleus (VM) | + | |
| *Septal* | Diagonal band nucleus (NDB) | ++ | + |
| | Lateral septum (LS) | + | +/- |
| | Medial septal nucleus (MS) | +++ | + |
| | Septofimbrial nucleus (SF) | +++ | ++ |
| | Triangular nucleus of septum (TRS) | +++ | ++ |

| | Region | Ipsi- | Contra- |
|---|---|---|---|
| *Amygdalar* | Anterior amygdalar area (AAA) | ++ | |
| | Basolateral amygdalar area (BLA) | +/- | |
| | Basomedial amygdalar nucleus (BMA) | ++ | |
| | Bed nucleus of stria terminalis (BST) | + | |
| | Central amygdalar nucleus (CEA) | +++ | |
| | Intercalated amygdalar nucleus (IA) | ++ | |
| | Medial amygdalar nucleus (MEA) | +++ | |
| *Olfactory* | Anterior olfactory nucleus (AON) | +++ | |
| | Cortical amygdala (CAA) | ++ | |
| | Dorsal peduncular area (DP) | ++ | + |
| | Main olfactory bulb (MOB) | +++ | |
| | Piriform cortex (PIR) | ++ | |
| | Taenia tecta (TT) | +++ | + |
| *Basal Ganglia* | Caudate putamen (CP) | +/- | |
| | Globus pallidus, external (GPe) | + | |
| | Nucleus accumbens, core (ACB) | +/- | |
| | Nucleus accumbens, shell (NAs) | +++ | |
| | Olfactory tubercle (OT) | +/- | |
| | Substantia nigra, compact (SNc) | + | |
| | Substantia nigra, reticulated (SNr) | +/- | |
| | Subthalamic nucleus (STN) | + | |
| *Hypothalamic* | Anterior hypothalamic nucleus (AHN) | ++ | + |
| | Dorsomedial hypothalamus (DMH) | ++ | |
| | Hypothalamic paraventricular nucleus (PVH) | + | + |
| | Lateral hypothalamic area (LHA) | +++ | + |
| | Lateral preoptic region (LPO) | + | |
| | Medial preoptic area (MPO) | ++ | + |
| | Median preoptic nucleus (MnPO) | + | + |
| | Posterior hypothalamic nucleus (PH) | ++ | + |
| | Suprachiasmatic nucleus (SCN) | +/- | |
| | Supramammillary nucleus (SUM) | ++ | + |
| | Ventrolatereal preoptic nucleus (VLPO) | + | |
| | Ventromedial hypothalamus (VMH) | +/- | |
| | Zona incerta (ZI) | ++ | + |
| *Midbrain/Pons* | Interpeduncular nucleus (IPN) | + | + |
| | Pedunculopontine nucleus (PPT) | + | |
| | Periaqueductal gray (PAG) | + | + |
| | Raphe, dorsal (DR) | + | + |
| | Raphe, medial (MR) | + | + |
| | Superior colliculus (SC) | +/- | |
| | Ventral tegmental area (VTA) | ++ | |

**Supplemental Table 2. Comprehensive list of BF Npas1$^{+}$ neuron ipsi- and contralateral projections within major brain regions and subregions**. +/-, minimal or ambiguous fibers. +, ++, +++, low, moderate, and high density of terminal fibers, respectively. The density of contralateral projections is reported if observed.

| Antigen | Immunizing Specificity | Host Species | Source/Cat. Number | Dilution | Refs. (Mouse brain tissue) | Antibody Registry # |
|---|---|---|---|---|---|---|
| ***Choline acetyltransferase (ChAT)*** | 68-kDa band on western blot assays<br><br>Source: Manufacturer; Bruce et al., 1995 | Goat | EMD Millipore AB144P | 1:200 | SI Refs. 21, 22 | AB_2079751 |
| ***Proto-oncogene c-Fos*** | ~60/56 kDa band observed in Western Blot assay.<br><br>Source: Manufacturer | Rabbit | EMD Millipore ABE457 | 1:200 | SI Refs. (23, 24) | AB_2631318 |
| ***Green Fluorescent Protein (GFP)*** | 27-kDa monomer of 238 amino acids<br><br>No detectable cross-reactivity with RFP<br><br>Source: Manufacturer | Mouse | EMD Millipore MAB3580 | 1:300 | SI Refs. (25-27) | AB_94936 |
| ***Neuronal PAS domain 1 (Npas1)*** | Validated in Npas1-cre-tomato and NPAS1 KO mice<br><br>(Hernandez et al., 2015) | Guinea Pig | Savio Chan (Northwestern Univ) | 1:1000 | SI Refs. (1, 16) | N/A |
| ***Parvalbumin (PV)*** | 12-kDa band on western blot assays<br><br>Source: Manufacturer | Sheep | RnD AF5058 | 1:150 | SI Refs. (28-30) | AB_2173907 |
| ***Red Fluorescent Protein (RFP)/DSRed*** | 30-38 kDa band on western blot assays<br><br>Source: Manufacturer | Rabbit | Takara 632496 | 1:1000 | SI Refs. (22, 31) | AB_10013483 |

**Supplemental Table 3**. Validation of primary antibodies.

| Secondary antibody | Vendor | Host Species | Catalog Number | Dilution | Incubation |
|---|---|---|---|---|---|
| *Donkey anti-mouse IgG AF488* | Thermo Fisher | Donkey | A21202 | 1:500 | 16 hrs 4ºC |
| *Donkey anti-goat IgG AF350* | Thermo Fisher | Donkey | A21081 | 1:100 | 4 hrs RT |
| *Donkey anti-goat IgG AF488* | Thermo Fisher | Donkey | A11015 | 1:100 | 4 hrs RT |
| *Donkey anti-guinea pig IgG AF488* | Jackson | Donkey | 706-545-148 | 1:500 | 2 hrs RT |
| *Donkey anti-guinea pig IgG AF594* | Jackson | Donkey | 706-585-148 | 1:500 | 2 hrs RT |
| *Donkey anti-rabbit IgG AF488* | Thermo Fisher | Donkey | A21206 | 1:200 | 2 hrs RT |
| *Donkey anti-rabbit IgG AF594* | Thermo Fisher | Donkey | A21207 | 1:100 | 2 hrs RT |
| *Donkey anti-sheep IgG AF350* | Thermo Fisher | Donkey | A21297 | 1:200 | 3 hrs RT |
| *Donkey anti-sheep IgG AF488* | Thermo Fisher | Donkey | A11015 | 1:200 | 3 hrs RT |

**Supplemental Table 4.** Secondary antibodies used in this study.

**SI References**


1. V.M. Hernandez *et al.*, Parvalbumin+ neurons and NPAS1+ neurons are distinct neuronal classes in the mouse external globus pallidus. *J. Neurosci.* **35(34)**, 11830-11847 (2015), 10.1523/JNEUROSCI.4672-14.2015.

2. J.A. Harris *et al.*, Anatomical characterization of Cre driver mice for neural circuit mapping and manipulation. *Front. Neural Circuits* **8**, 76 (2014), 10.3389/fncir.2014.00076.

3. M. Krenzer *et al.*, Brainstem and spinal cord circuitry regulating rem sleep and muscle atonia. *PLoS One* **6(10)**, e24998 (2011), 10.1371/journal.pone.0024998.

4. L. Vong *et al.*, Leptin action on GABAergic neurons prevents obesity and reduces inhibitory tone to POMC neurons. *Neuron* **71(1)**, 142-154 (2011), 10.1016/j.neuron.2011.05.028.

5. C. Anaclet *et al.*, Basal forebrain control of wakefulness and cortical rhythms. *Nat. Commun.* **6**, 8744 (2015), 10.1038/ncomms9744.

6. J.T. McKenna *et al.*, Characterization of basal forebrain glutamate neurons suggests a role in control of arousal and avoidance behavior. *Brain Struct. Funct.* **226(6)**, 1755-1778 (2021), 10.1007/s00429-021-02288-7.

7. N. Tamamaki *et al.*, Green fluorescent protein expression and colocalization with calretinin, parvalbumin, and somatostatin in the GAD67-GFP knock-in mouse. *J. Comp. Neurol.* **467(1)**, 60-79 (2003), 10.1002/cne.10905.

8. R.E. Brown *et al.*, Characterization of GABAergic neurons in rapid-eye-movement sleep controlling regions of the brainstem reticular formation in GAD67-green fluorescent protein knock-in mice. *Eur. J. Neurosci.* **27(2)**, 352-63 (2008), 10.1111/j.1460-9568.2008.06024.

9. J.T. McKenna *et al.*, Distribution and intrinsic membrane properties of basal forebrain GABAergic and parvalbumin neurons in the mouse. *J. Comp. Neurol.* **521**, 1225-1250 (2013), 10.1002/cne.23290.

10. C. Yang *et al.*, Cholinergic neurons excite cortically projecting basal forebrain GABAergic neurons. *J. Neurosci.* **34(8)**, 2832-2844 (2014), 10.1523/JNEUROSCI.3235-13.2014.

11. D.B. Rye, B.H. Wainer, M.M. Mesulam, E.J. Mufson, C.B. Saper, Cortical projections arising from the basal forebrain: a study of cholinergic and noncholinergic components employing combined retrograde tracing and immunohistochemical localization of choline acetyltransferase. *Neuroscience* **13(3)**, 627-643 (1984), 10.1016/0306-4522(84)90083-6.

12. I. Gritti, I.D. Manns, L. Mainville, B.E. Jones, Parvalbumin, calbindin, or calretinin in cortically projecting and GABAergic, cholinergic, or glutamatergic basal forebrain neurons of the rat. *J. Comp. Neurol.* **458(1)**, 11-31 (2003), 10.1002/cne.10505.

13. P. Henny, B.E. Jones, Projections from basal forebrain to prefrontal cortex comprise cholinergic, GABAergic and glutamatergic inputs to pyramidal cells or interneurons. *Eur. J. Neurosci.* **27(3)**, 654-670 (2008), 10.1111/j.1460-9568.2008.06029.x.

14. J.P. Do *et al.,* Cell type-specific long-range connections of basal forebrain circuit. *Elife* **5**, e13214 (2016), 10.7554/eLife.13214.

15. K.B.J. Franklin, G. Paxinos, The mouse brain in stereotaxic coordinates. New York: Academic Press (2008).

16. Z.A. Abecassis et al., Npas1+-Nkx2.1+ neurons are an integral part of the cortico-pallidal-cortical loop. *J. Neurosci.* **40(4)**, 743-768 (2020), 10.1523/JNEUROSCI.1199-19.2019.

17. J.T. McKenna *et al.,* Basal forebrain parvalbumin neurons mediate arousals from sleep induced by hypercarbia or auditory stimuli. *Curr. Biol.* **30(12)**, 2379-2385 (2020), 10.1016/j.cub.2020.04.029.

18. D.S. Uygun *et al.,* Knockdown of GABAA alpha3 subunits on thalamic reticular neurons enhances deep sleep. *Nat. Commun.* **13**, 2246 (2022), 10.1038/s41467-022-29852-x.

19. D.S. Uygun *et al.,* Validation of an automated sleep spindle detection method for mouse EEG. *SLEEP* **42(2)**, zsy218 (2019), 10.1093/sleep/zsy218.

20. M.J. Prerau, R.E. Brown, M.T. Bianchi, J.M. Ellenbogen, P.L. Purdon, Sleep Neurophysiological Dynamics Through the Lens of Multitaper Spectral Analysis. *Physiology* **32(1)**, 60-92 (2017), 10.1152/physiol.00062.2015.

21. A. Sanz-Diez, M. Najac, D. De Saint Jan, Basal forebrain GABAergic innervation of olfactory bulb periglomerular interneurons. *J. Physiol.* **597(9)**: 2547-2563 (2019), 10.1113/JP277811.

22. F. Grady, L. Peltekian, G. Iverson, J.C. Geerling, Direct Parabrachial-Cortical Connectivity. *Cereb. Cortex* **30(9)**, 4811-4833 (2020), 10.1093/cercor/bhaa072.

23. Y. Takata *et al.,* Sleep and wakefulness are controlled by ventral medial midbrain/pons GABAergic neurons in mice. *J. Neurosci.* **38(47)**, 10080-10092 (2018), 10.1523/JNEUROSCI.0598-19.2018.

24. X.-S. Yuan *et al.,* Striatal adenosine A2a receptor neurons control active-period sleep via parvalbumin neurons in external globus pallidus. *Elife* **6**, e29055 (2017), 10.7554/eLife.29055.

25. J. Helgager, G. Liu, J.O. McNamara, The cellular and synaptic location of activated TrkB in mouse hippocampus during limbic epileptogenesis. *J. Comp. Neurol.* **521**, 499-521 (2013), 10.1002/cne.23225.

26. Y.S. Jo, G. Heymann, L.S. Zweifel, Dopamine neurons reflect the uncertainty in fear generalization. *Neuron* **100(4)**, 916-925 (2018), 10.1016/j.neuron.2018.09.028.

27. S. Thankachan *et al.*, Thalamic reticular nucleus parvalbumin neurons regulate sleep spindles and electrophysiological aspects of schizophrenia in mice. *Sci. Rep.* **9(1)**, 3607 (2019), 10.1038/s41598-019-40398-9.

28. T. Iijima, Y. Iijima, H. Witte, P. Scheiffele, Neuronal cell-type specific alternative splicing is regulated by the KH domain protein SLM1. *J. Cell Biol.* **204(3)**, 331-342 (2014), 10.1083/jcb.201310136.

29. D. Usoskin *et al.*, Unbiased classification of sensory neuron types by large scale single-cell RNA sequencing. *Nat. Neurosci.* **18(1)**, 145-153 (2015), 10.1038/nn.3881.

30. C. Stephany *et al.*, Plasticity of binocularity and visual acuity are differentially limited by nogo receptor. *J. Neurosci.* **34(35)**, 11631-11640 (2014), 10.1523/JNEUROSCI.0545-14.2014.

31. T.R. Pardo-Garcia, Ventral Pallidum is the primary target for accumbens D1 projections driving cocaine seeking. *J. Neurosci.* **39(11)**, 2041-2051 (2019), 10.1523/JNEUROSCI.2822-18.2018.